

Low-energy p-d Scattering: High Precision Data, Comparisons with Theory, and Phase-Shift Analyses

M. H. Wood*, C. R. Brune, B. M. Fisher, H. J. Karwowski, D. S. Leonard, and
E. J. Ludwig

*Department of Physics and Astronomy, University of North Carolina at Chapel Hill
Chapel Hill, NC 27599-3255, USA
and Triangle Universities Nuclear Laboratory, Durham, NC 27088-0308, USA*

A. Kievsky, S. Rosati, and M. Viviani

*Istituto Nazionale di Fisica Nucleare, Sezione di Pisa and Dipartimento di Pisa, Università di
Pisa, I-56100 Pisa, Italy*

(October 27, 2018)

Abstract

Angular distributions of $\sigma(\theta)$, A_y , iT_{11} , T_{20} , T_{21} , and T_{22} have been measured for d-p scattering at $E_{c.m.} = 667$ keV. This set of high-precision data is compared to variational calculations with the nucleon-nucleon potential alone and also to calculations including a three-nucleon (3N) potential. Agreement with cross-section and tensor analyzing power data is excellent when a 3N potential is used. However, a comparison between the vector analyzing powers reveals differences of approximately 40% in the maxima of the angular distributions which is larger than reported at higher energies for both p-d and n-d scattering. Single-energy phase-shift analyses were performed on this data set and a similar data set at $E_{c.m.} = 431.3$ keV. The role of the different phase-shift parameters in fitting these data is discussed.

PACS number(s): 13.75.Cs, 21.45.+v, 24.70.+s, 21.30.Fe

Typeset using REVTeX

*Present Address: Thomas Jefferson National Accelerator Facility, 12000 Jefferson Ave., Newport News, VA, 23606

I. INTRODUCTION

An important question in low-energy nuclear physics is whether a nucleon-nucleon (NN) interaction is sufficient to describe few-nucleon systems or whether a three-nucleon force (3NF) is necessary when the system consists of $A \geq 3$. To solve for the bound and scattering states of the three-nucleon (3N) system, state-of-the-art theoretical methods like the Faddeev method [1] (which works well for n-d scattering) have been developed. It was not until the advancement of variational techniques [2] which could include the Coulomb force rigorously that serious comparisons could be made with p-d scattering data. Current theoretical investigations incorporate phenomenological NN potentials such as CD Bonn [3], Nijmegen III [4], and Argonne v_{18} (AV18) [5]. These potentials are based on the one-pion-exchange potential for large interparticle separations as well as fits to the present NN database. When calculations using those models are performed in the three-nucleon system, the ${}^3\text{He}$ and ${}^3\text{H}$ binding energies are underestimated by approximately 0.5 to 1.0 MeV depending on which NN potential is employed. The under-prediction of the $A = 3$ binding energies is the first indication that the two-nucleon interaction alone, as parameterized by the NN potentials in their current forms, is insufficient for an accurate description of the 3N data. To remedy the situation, phenomenological 3N potentials such as the Tucson-Melbourne (TM) [6], the Brazil (BR) [7], and the Urbana IX (UR-IX) [8] were introduced which are based on the 2π exchange interaction and adjusted to reproduce the triton binding energies. By applying chiral-perturbation theory to the 3NFs, Friar *et al.* [9] showed that the present phenomenological 3NFs are equivalent to first-order in the Lagrangian they constructed except for one term in the TM potential which was found to be of next-to-leading order.

Beyond the binding-energy problem, there is another large discrepancy in the properties of the 3N system, namely the vector analyzing powers (VAPs) A_y and iT_{11} for N-d scattering. Comparisons between variational calculations [10] including one of the NN potentials and VAP measurements at $E_{c.m.} \leq 2$ MeV [11,12] show that the calculations under-predict the data by $\approx 30\%$ in the maximum of the angular distributions. The disagreement becomes worse at lower energies where the difference increases to $\approx 40\%$ at $E_{c.m.} = 431.3$ keV [13,14]. This VAP problem was first observed for A_y in n-d scattering and has been labelled the “ A_y puzzle” [15,16]. The trend of the “ A_y puzzle” for both A_y and iT_{11} is a decreasing discrepancy as the energy increases as shown in Fig. 1. The disagreement mostly disappears at $E_{c.m.} \approx 30$ MeV [17]. The inclusion of a 3NF in the variational calculations lessens the discrepancies with A_y and iT_{11} data for p-d scattering at the aforementioned energies by no more than 15%. The effect of the magnetic moments was investigated by Stoks [18] and found not to provide the solution.

To investigate this question further, we have measured with high precision A_y and iT_{11} as well as the cross section $\sigma(\theta)$ and the tensor analyzing powers (TAPs) T_{20} , T_{21} , T_{22} for p-d elastic scattering at $E_{c.m.} = 667$ keV. To isolate the deficient phase shifts and mixing parameters in the theoretical calculations, two single-energy phase-shift analyses are performed, one with these data at $E_{c.m.} = 667$ keV and another with the same observables at $E_{c.m.} = 431.3$ keV [13,14,19,20] previously measured by our group. Additional information concerning the experimental details and analysis is available in Ref. [21]. Moreover, the 667 keV cross-section measurement was included in a χ^2 study [22] with other cross-section data below $E_{c.m.} = 2$ MeV.

II. EXPERIMENTAL DETAILS

The basic experimental setup and techniques were developed for our measurements of d-p elastic scattering at $E_{c.m.} = 431.3$ keV and are described in Ref. [13,14,19–22]. The modifications to the setup described in Ref. [14] for the experiments conducted at $E_{c.m.} = 667 \pm 1$ keV will be discussed. One advantage of making measurements at $E_{c.m.} = 667$ keV over 431.3 keV is the reduction of the Rutherford scattering of the incident particles from carbon which was present in the targets. The statistical uncertainties in this set of measurements are significantly smaller than in the measurement at 431.3 keV. The only slight disadvantage is the presence of additional proton groups from the $^{12}\text{C}(d,p)^{13}\text{C}$ reaction in the deuteron beam experiments. All six angular distribution measurements employed the FN tandem accelerator at the Triangle Universities Nuclear Laboratory to give a deuteron (proton) beam energy in the center of the target of 2.00 MeV (1.00 MeV).

A. Cross-Section Measurements

The relative cross-section was measured with a beam of deuterons on thin hydrogenated carbon targets [23] which contained approximately $(0.5 \pm 0.1) \times 10^{18}$ H/cm² and $(1.0 \pm 0.2) \times 10^{18}$ C/cm². The rest of the experimental details can be found in Ref. [22]. A sample spectrum for $^1\text{H}(d,d)^1\text{H}$ scattering at $\theta_{lab} = 26.1^\circ$ is shown in Fig. 2. The absolute cross-section was obtained by normalizing the relative $\sigma(\theta)$ for d-p scattering to the well-known $^1\text{H}(p,p)^1\text{H}$ cross-section determined by the Nijmegen phase-shift analysis [24]. The uncertainties of the absolute cross-section measurement are 0.5% from counting statistics, 0.5% from the normalization to the p-p scattering cross-section, and 0.6% from the beam-current integration. The absolute $\sigma(\theta)$ angular distributions are shown in Fig. 3a. The data are divided by the results of the variational calculation to emphasize the differences between the data and the calculations.

B. Analyzing Power Measurements

For the five analyzing power measurements, the techniques used were similar to those described in Refs. [13,14]. The targets [23] contained $(1.0 \pm 0.2) \times 10^{18}$ hydrogen or deuterium atoms and $(2.0 \pm 0.4) \times 10^{18}$ carbon atoms per cm². The beam polarization for each experiment was measured online with a polarimeter situated behind the scattering chamber. For the T_{20} , T_{21} , and T_{22} experiments, a polarimeter [25] based on the $^3\text{He}(\vec{d},p)^4\text{He}$ reaction was utilized. The beam polarizations for the T_{20} and T_{22} measurements were $p_{zz} \approx \pm 0.8$ and $p_{zz} \approx 0$ for the three spin states with a 3% error. For the T_{21} measurement, the beam polarizations were $p_{zz} \approx \pm 0.8$ and $p_{zz} \approx 0$ with a 2% error. For iT_{11} , a polarimeter [21] based on the $^2\text{H}(\vec{d},p)^3\text{H}$ reaction was used, and the beam polarizations were $p_z \approx \pm 0.55$. For the proton beam, the $^6\text{Li}(\vec{p},^3\text{He})^4\text{He}$ reaction [21,26] was employed for polarimetry. The beam polarization over the duration of the experiment was $p_z \approx \pm 0.65$. The error in the beam polarizations for both experiments was 2%.

The coincidence technique described in Ref. [13] was used for the VAP experiments. A new addition was 2- μm -thick mylar foils that were placed in front of the detectors to block

any heavy recoil particles such as carbon atoms. By making the measurements at the higher energy, it was possible to cover a larger angular range ($\theta_{c.m.} \approx 50^\circ - 140^\circ$) than obtained at 431.3 keV. A typical timing spectrum for p-d coincidences for a deuteron beam incident on a hydrogen target is shown in Fig. 4. The TAP and VAP angular distributions are given in Figs. 3 and 5, respectively.

III. COMPARISONS WITH THE THEORETICAL CALCULATIONS

Theoretical calculations to compare with the data have been produced using the AV18 potential and the AV18 plus a 3NF. These calculations employ the Pair-Correlated Hyperspherical Harmonic basis to construct the scattering wave functions and the Kohn variational principle to solve for the scattering-matrix elements [2]. In order to study the sensitivity to different 3NF models, the UR-IX, the TM and its modified version denoted TM' interactions have been considered. Originally the TM potential [6] was given as a sum of four terms characterized by the strengths a, b, c, d . To assure consistency with chiral symmetry the a -term in the TM model has been redefined with a new constant $a' = a - 2m_\pi^2 c$ (which essentially implies a change of sign for the constant a) and the c -term has been set to zero [9]. The TM' model, as well as the TM and the UR-IX potentials, have been used recently in an extensive study of 3NF effects in n-d scattering above $E_{c.m.} = 2$ MeV [27]. For completeness, here we will present results using the same set of constants as Ref. [27] for the TM and TM' models.

Accompanying the data presented in Figs. 3 and 5 are several separate variational calculations, one including the AV18 potential and the others with the AV18 and either the UR-IX or TM potentials. It is clear that the calculations with or without the 3N potential reproduce $\sigma(\theta)$ and the TAP data fairly well. On the other hand, the agreement with the VAP data is much poorer. These results are qualitatively similar to those observed at higher energies which were mentioned in the Introduction. For the present case, the differences between the NN-potential-only calculations and the A_y and iT_{11} measurements are approximately 40% and 37%, respectively at the maximum of the angular distributions. With the inclusion of the UR-IX potential, the agreement for all of the observables improves; however, the change in the VAPs is only marginal and a large discrepancy still remains on the order of 36% and 29% for A_y and iT_{11} , respectively. When the TM 3N-potential is included, the VAP calculations show slightly worse agreement with the data (39% and 34% differences) than in the case of the UR-IX potential. However, when the TM' potential is used, the calculations are closer to the VAP data than for the case of the UR-IX potential; the difference between $A_y(iT_{11})$ data and the calculations is 32%(25%). The same trend has been observed in Ref. [27] at $E_{c.m.} = 2$ MeV. The difference between the calculations with the TM' potential and those with UR-IX is about 5%. While each of the 3NFs mentioned here provide some improvement to the A_y and iT_{11} calculations, none of the potentials eliminates the discrepancy. To obtain a more quantitative comparison, the reduced χ^2 , χ_N^2 , was calculated for each observable, and the results are described in Sec. IV.

Besides the TM' potential, other modified NN and 3N force models have recently become available. For example, a new NN interaction constructed from chiral perturbation theory seems to give a better description of the VAP data at low energy [28]. A different possibility may be in the construction of a new 3N force. Hüber and Friar [29] have suggested that a possible candidate should be a spin-dependent 3NF since the VAP is a difference between

polarized cross-sections. Following this direction, a phenomenological 3N $\vec{L} \cdot \vec{S}$ force has recently been proposed [30]. This new force essentially modifies the scalar function $v_{11}^{ls}(r)$ already present in the $\vec{L} \cdot \vec{S}$ term of the AV18 potential in triplet spin and isospin channels. Explicitly the following form has been proposed

$$V_{3N}^{ls} = \sum_{i < j} v_{11}^{ls}(r_{ij}) \mathbf{L}_{ij} \cdot \mathbf{S}_{ij} P_{11}(ij) + W_0 e^{-\alpha \rho} \sum_{i < j} \mathbf{L}_{ij} \cdot \mathbf{S}_{ij} P_{11}(ij). \quad (1)$$

where P_{11} is a projector in channels with spin $S_{ij} = 1$ and isospin $T_{ij} = 1$. The hyperradius ρ is

$$\rho = \sqrt{\frac{2}{3}(r_{12}^2 + r_{23}^2 + r_{31}^2)} \quad (2)$$

and W_0 and α are parameters characterizing the strength and range of the three-body term. This force influences the splitting of the 4P_J phases and the magnitude of $\epsilon_{3/2-}$ without appreciably affecting the other parameters. Moreover, when the deuteron and spectator nucleon are separated by a large distance, the proposed interaction reduces to the original NN $\vec{L} \cdot \vec{S}$ potential $v_{11}^{ls}(r_{ij})$. Fig. 6 shows A_y and iT_{11} calculated using this new potential for three different strength and range parameters. The values for W_0 and α have been taken from Ref. [30] and have been fixed in order to reproduce the VAP data at $E_{c.m.} = 2$ MeV. The addition of the 3N spin-orbit force has provided much better agreement with our VAP data than previous calculations. The various phase-shift parameters will be discussed in detail in Sec. V. Moreover the calculated differential cross sections and TAPs remain essentially unchanged [30] by the new term.

IV. CALCULATIONS OF REDUCED χ^2

To investigate quantitatively the effects of the UR-IX potential, reduced χ^2 calculations were completed with both the AV18 potential and the AV18+UR-IX potentials. More details for the $\sigma(\theta)$ comparison are presented in Ref. [22], and the results are listed in the first two lines of Table I. None of the data were renormalized in order to find a minimal χ_N^2 . From χ_N^2 calculations, it is possible to draw conclusions similar to those from the visual comparisons: the $\sigma(\theta)$ and the TAP data are reproduced very well while VAP data show poorer agreement with theory. However, all of the χ_N^2 are improved when a 3NF is included. For $\sigma(\theta)$, χ_N^2 improves by an order of magnitude. The χ_N^2 is reduced significantly for each TAP. The calculations of A_y and iT_{11} with UR-IX show improved agreement with the data; however, the χ_N^2 remains in the hundreds.

V. PHASE-SHIFT ANALYSIS

The technique of Phase Shift Analysis (PSA) is useful for determining the dependences of the observables on the various partial waves, and also for studying the sources of disagreements between theory and experiment. Here we consider data at two energies: $E_{c.m.} = 667$ keV, the energy of the present data, and also $E_{c.m.} = 431.3$ keV, the energy of previous measurements in our laboratory [14]. The PSAs reported here are carried out in

the framework of Seyler [31], where the scattering matrix is parameterized in terms of phase shifts and mixing parameters. The phase shift parameters in general depend on orbital angular momentum L , total angular momentum J , and the channel spin S . The mixing parameters connect partial waves with different L and/or S for a given J and parity.

Before embarking upon a detailed PSA, it is important to understand the convergence of the observables versus the angular momentum cutoff. Studies were performed using the AV18+UR-IX calculations for the phase shifts and mixing parameters. The dependence on the angular momentum cutoff L_{max} was examined by setting to zero all phase shifts and mixing parameters with $L > L_{max}$ for different values of L_{max} . Note that the effect of the Coulomb potential is retained in all partial waves, so it is expected that the observables will converge quickly. We have quantified the convergence of the observables by using χ_N^2 comparisons of the calculations with different L_{max} values to the experimental data at $E_{c.m.} = 431.3$ and 667 keV. The results are shown in Table II. First of all we find very little change in χ_N^2 between $L_{max} = 3$ and $L_{max} = 4$, indicating, as expected, that the results are already well-converged with $L_{max} = 3$ at these low energies. It is also interesting to note that the cross section and TAPs are fairly well described with $L_{max} = 2$, while only $L_{max} = 1$ is required to produce a similar level of convergence for the VAPs. Smaller, but statistically-significant improvements are obtained by extending to $L_{max} = 3$. We have also observed in these studies that the observables T_{20} and T_{22} are highly dependent on the $L = 2$ phase shifts and mixing parameters.

Single-energy PSAs have been performed by using the phase shifts and mixing parameters produced by the AV18+UR-IX potential as starting values. Some of the parameters are allowed to vary freely; the best-fit values for the variable parameters are determined by χ^2 minimization with attention given to the fitting procedure to avoid local minima. Phase shifts were included up to a maximum angular momentum of $L = 4$, but only those with $L \leq 2$ were allowed to vary.

Previous phase-shift analyses [10,11] have linked the VAP problem to the P -wave phase-shifts. To test the effects of the different P -wave phase-shifts and their associated mixing parameters, two-parameter fits were made. Tables I and III show the χ_N^2 at the two energies for sample trials where only the P -wave phase-shifts were varied. By varying the 2P_J phase-shifts and/or the mixing parameter $\epsilon_{1/2-}$ freely (trials 1 and 2), there is very little change in the χ_N^2 with the exception of iT_{11} at 431.3 keV. With the combination of $\epsilon_{3/2-}$ and a 4P_J phase-shift (trials 3, 4, and 5), good fits were produced with the most dramatic improvement occurring in each VAP. At $E_{c.m.} = 667$ keV, the χ_N^2 reduced by a factor of approximately 300 for A_y and a factor of 30 for iT_{11} . For the $E_{c.m.} = 431.3$ keV case, the fits produced reductions in χ_N^2 by factors of approximately 20 and 10 for A_y and iT_{11} , respectively, with the exception of the fit to iT_{11} with the free parameters ${}^4P_{3/2}$ and $\epsilon_{3/2-}$. A comparison of the three 4P_J trials indicates that the two-parameter fit with the ${}^4P_{1/2}$ phase-shift and $\epsilon_{3/2-}$ gives the best result although the differences with the other two trials are very small. These trials so far illustrate the influence of the P -wave phase-shifts and $\epsilon_{3/2-}$; however, a more realistic fit (trial 6) is to allow all of the S - and P -wave phase-shifts with $\epsilon_{1/2-}$ and $\epsilon_{3/2-}$ to vary freely (9 parameters in all). The remaining phases and mixing parameters were taken from the AV18+UR-IX calculations [10]. The results of the fits are listed in Table IV.

While there were improvements with the full S - and P -wave fits over the two parameter 4P_J fits, the reduction in χ_N^2 is small. To make a more quantitative comparison between

trials, errors were determined for specific parameters by the change in a specific parameter necessary to increase the minimal χ^2 by 1 [32]. Allowing more parameters to vary led to a larger error in each parameter which underlies our attempts to find the best fit with the least number of parameters. The uncertainties in phase shifts and mixing parameters when all S - and P -wave parameters were varied are given in Table IV. These errors reflect the contribution of statistical uncertainties in the data only.

The PSA presented here produced very good fits to the data sets at $E_{c.m.} = 431.3$ keV and 667 keV with sensible results. The greatest influence on the A_y and iT_{11} fits came from the 4P_J phase-shifts and $\epsilon_{3/2^-}$ parameter. This result was noticed in the earlier analyses [10,11] at higher energies. It is difficult to provide a more precise value from the PSA for each phase-shift with the present data sets at 431.3 keV and 667 keV. What these analyses do confirm is the need to modify the 4P_J phase-shifts and the mixing between the ${}^4P_{3/2}$ and the ${}^2P_{3/2}$ phase-shifts (as evident from the change in $\epsilon_{3/2^-}$). In fact, $\epsilon_{3/2^-}$ was increased (in absolute value) by about 19% from the 667 keV PSA and by about 28% from the 431.3 keV PSA over the predicted value even when the UR-IX potential was included in the calculations. The reader should be cautioned that the errors from both analyses allow much wider ranges of values for $\epsilon_{3/2^-}$. The theoretical calculations also appear to underestimate the splitting $\Delta P = {}^4P_{5/2} - {}^4P_{1/2}$. For example at 667 keV the calculated splitting is $\Delta P = 0.87^\circ$ compared to 0.96° obtained in the fit. At 431.3 keV the difference is even bigger; the calculated value is $\Delta P = 0.48^\circ$ compared to 0.63° from the fit. The small, but nevertheless important, underestimation of ΔP has been found also in the calculations at $E_{c.m.} = 2$ MeV [10].

VI. CONCLUSIONS

In conclusion, we have presented high-precision measurements of $\sigma(\theta)$, A_y , iT_{11} , T_{20} , T_{21} , and T_{22} for p-d elastic scattering at a center-of-mass energy of 667 keV. The cross section and TAP data show excellent agreement with the variational calculations using the AV18 and UR-IX potentials. The “ A_y puzzle” persists at this energy with the inclusion of the UR-IX in the calculations giving a small improvement in the agreement with the VAP data. In order to extend the analysis to different forms of the 3NFs, the AV18+TM and AV18+TM’ potential models have also been considered in the comparisons to the data. The calculations with either TM potential under-predict the VAP data by a similar amount as in the case of the AV18+UR-IX results. From the reduced χ^2 analysis, it is clear that adding a 3NF into the calculations improves the agreement with the data for all of the observables.

From a single-energy PSA at very low energies ($E_{c.m.} = 431.3$ keV and 667 keV), the under-prediction of the VAP data by the calculations appears to be caused by certain P -wave components. By varying two parameters, $\epsilon_{3/2^-}$ and one of the 4P_J phase-shifts, and maintaining all of the other parameters as determined from theory, an almost perfect fit was achieved for A_y . For iT_{11} , the χ_N^2 was reduced by more than an order of magnitude to approximately 1.3 for the 431.3 keV PSA and 1.8 for the 667 keV analysis. To obtain an even better fit, all of the S - and P -wave phase-shifts along with $\epsilon_{1/2^-}$ and $\epsilon_{3/2^-}$ were varied freely to obtain χ_N^2 of ≈ 1.0 for each observable. The results of this analysis are the same within the errors as the PSA with $\epsilon_{3/2^-}$ and a 4P_J phase-shift as the only free parameters. From comparisons of the PSA results to calculations it is evident that the theory underestimates the splitting of the 4P_J phase shifts as well as the mixing between ${}^2P_{3/2}$ and ${}^4P_{3/2}$.

The inclusion of a phenomenological 3N spin-orbit force, which fixes the P -wave mixing in the calculations, provides better agreement with the VAP data without disturbing the agreement obtained for the cross-section and TAP data. While this fact does not determine the existence of a 3NF, it indicates a need to develop and refine the current 3N potential models [38]. In addition, one can not rule out the possibility that currently employed NN 3P_J interactions are incorrect [28].

Finally, the A_y problem can be studied with information from p- ${}^3\text{He}$ elastic scattering data. The variational calculations employed in this paper have recently been extended to the p- ${}^3\text{He}$ scattering observables [39]. In this case there is an underprediction by approximately 40% of new A_y data taken at an $E_{c.m.}$ below 2 MeV. Moreover, A_y for p- ${}^3\text{He}$ scattering is an order of magnitude larger than for the p-d scattering case. This fact makes it an ideal candidate for future investigations, and more p- ${}^3\text{He}$ elastic scattering data at low energies is needed.

ACKNOWLEDGMENTS

The authors would like to thank Dr. K. D. Veal for his assistance in the data taking. This work was supported in part by the US DOE under Grant No. DE-FG02-97ER41041.

REFERENCES

- [1] W. Glöckle, *The Quantum Mechanical Few-Body Problem*, Lecture Notes in Physics Vol. 273, Springer-Verlag, Berlin (1983).
- [2] A. Kievsky, M. Viviani, and S. Rosati, Nucl. Phys. **A577**, 511 (1994).
- [3] M. F. Jiang, R. Machleidt, D. B. Stout, and T. T. S. Kuo, Phys. Rev. C **46**, 910 (1992).
- [4] V. G. J. Stoks, R. A. M. Klomp, C. P. F. Terheggen, and J. J. de Swart, Phys. Rev. C **49**, 2950 (1994).
- [5] R. B. Wiringa, V. G. J. Stoks, and R. Schiavilla, Phys. Rev. C **51**, 38 (1995).
- [6] S. A. Coon, M. D. Scadron, P. C. McNamee, B. R. Barrett, D. W. E. Blatt, and B. H. J. McKellar, Nucl. Phys. **A317**, 242 (1979).
- [7] H. T. Coelho, T. K. Das, and M. R. Robilotta, Phys. Rev. C **28**, 1812 (1983).
- [8] B. S. Pudliner, V. R. Pandharipande, J. Carlson, and R. B. Wiringa, Phys. Rev. Lett. **74**, 4396 (1995).
- [9] J. L. Friar, D. Hüber, and U. van Kolck, Phys. Rev. C **59**, 53 (1999).
- [10] A. Kievsky, S. Rosati, W. Tornow, and M. Viviani, Nucl. Phys. **A607**, 402 (1996).
- [11] L. D. Knutson, L. O. Lamm, and J. E. McAninch, Phys. Rev. Lett. **71**, 3762 (1993).
- [12] S. Shimizu, K. Sagara, H. Nakamura, K. Maeda, T. Miwa, N. Nishimori, S. Ueno, T. Nakashima, and S. Morinobu, Phys. Rev. C **52**, 1193 (1995).
- [13] C. R. Brune, W. H. Geist, H. J. Karwowski, E. J. Ludwig, K. D. Veal, M. H. Wood, A. Kievsky, S. Rosati, and M. Viviani, Phys. Lett. B **428**, 13 (1998).
- [14] C. R. Brune, W. H. Geist, H. J. Karwowski, E. J. Ludwig, K. D. Veal, M. H. Wood, A. Kievsky, S. Rosati, and M. Viviani, Phys. Rev. C **63**, 044013 (2001).
- [15] W. Tornow, C. R. Howell, M. Alohal, Z. P. Chen, P. D. Felsher, J. M. Hanly, R. L. Walter, G. Mertens, I. Slaus, H. Witala, and W. Glöckle, Phys. Lett. B **257**, 273 (1991).
- [16] H. Witala and W. Glöckle, Nucl. Phys. **A528**, 48 (1991); H. Witala, D. Hüber, and W. Glöckle, Phys. Rev. C **49**, R14 (1994).
- [17] W. Glöckle, H. Witala, D. Hüber, H. Kamada, and J. Golak, Phys. Rep. **274**, 107 (1996).
- [18] V. G. J. Stoks, Phys. Rev. C **57**, 445 (1998).
- [19] A. Kievsky, S. Rosati, M. Viviani, C. R. Brune, H. J. Karwowski, E. J. Ludwig, and M. H. Wood, Phys. Lett. B **406**, 292 (1997).
- [20] H. J. Karwowski, C. R. Brune, W. H. Geist, E. J. Ludwig, K. D. Veal, M. H. Wood, A. Kievsky, S. Rosati, M. Viviani, and T. C. Black, Acta Physica Polonica B **30**, 1479 (1999).
- [21] M. H. Wood, Ph.D. thesis, University of North Carolina at Chapel Hill (2000).
- [22] A. Kievsky, M. H. Wood, C. R. Brune, B. M. Fisher, H. J. Karwowski, D. S. Leonard, E. J. Ludwig, S. Rosati, and M. Viviani, Phys. Rev. C **63**, 024005 (2001).
- [23] T. C. Black, Ph.D. thesis, University of North Carolina at Chapel Hill (1995), Available from University Microfilms, Ann Arbor, Michigan, order #9616149.
- [24] V. G. J. Stoks, R. A. M. Klomp, M. C. M. Rentmeester, and J. J. de Swart, Phys. Rev. C **48**, 792 (1993); M. C. M. Rentmeester and J. J. de Swart, preliminary Nijmegen proton-proton PWA97 (private communication).
- [25] S. A. Tonsfeldt, *Polarization Phenomena in Nuclear Physics*, Part 2, Santa Fe, NM, AIP, 961 (1980); S. A. Tonsfeldt, Ph.D. thesis, University of North Carolina at Chapel Hill, Available from University Microfilms, Ann Arbor, Michigan, order #8022515.

- [26] C. R. Brune, H. J. Karwowski, and E. J. Ludwig, Nucl. Instrum. Methods A **389**, 421 (1997).
- [27] H. Witala, W. Glöckle, J. Golak, A. Nogga, H. Kamada, R. Skibiński, and J. Kuroszolnierzuk, Phys. Rev. C **63**, 024007 (2001).
- [28] E. Epelbaum, H. Kamada, A. Nogga, H. Witala, W. Glöckle, and Ulf-G. Meissner, Phys. Rev Lett. **86**, 4787 (2001).
- [29] D. Hüber and J. L. Friar, Phys. Rev. C **58**, 674 (1998).
- [30] A. Kievsky, Phys. Rev. C **60**, 034001 (1999).
- [31] R. G. Seyler, Nucl. Phys. **A124**, 253 (1969).
- [32] P. R. Bevington and D. K. Robinson, *Data Reduction and Error Analysis for the Physical Sciences*, second edition, McGraw-Hill, New York (1992).
- [33] K. Sagara, H. Oguri, S. Shimizu, K. Maeda, H. Nakamura, T. Nakashima, and S. Morinobu, Phys. Rev. C **50**, 576 (1994).
- [34] K. Sagara, private communication.
- [35] J. Sowinski, D. D. Pun Casavant, and L. D. Knutson, Nucl.Phys. **A464**, 223 (1987).
- [36] W. Grüebler, V. König, P. A. Schmelzbach, F. Sperisen, B. Jenny, R. E. White, F. Seiler, and H. W. Roser, Nucl. Phys. **A398**, 445 (1983).
- [37] E. Huttel, W. Arnold, H. Berg, H. H. Krause, J. Ulbright, and G. Clausnitzer, Nucl. Phys. **A406**, 435 (1983).
- [38] W. Shadow and L. Canton, Phys. Rev. C, in press.
- [39] M. Viviani, A. Kievsky, S. Rosati, E. A. George, and L. D. Knutson, Phys. Rev. Lett. **86**, 3739 (2001).

TABLES

TABLE I. The χ_N^2 calculated for each trial of the phase-shift analysis for each observable measured at $E_{c.m.} = 667$ keV. The number of data points in the angular distribution of each observable is the value in parentheses under the title. The total χ_N^2 is the sum of χ^2 for each observable divided by 143 (the total number of data points).

Trial	Free Parameters	χ_N^2						Total (143)
		$\sigma(\theta)$ (56)	A_y (7)	iT_{11} (8)	T_{20} (24)	T_{21} (24)	T_{22} (24)	
AV18	None	45.2	275.8	112.4	3.5	3.5	2.8	39.3
AV18+UR	None	1.2	190.5	61.4	1.0	2.5	0.7	13.9
1	${}^2P_{1/2}, {}^2P_{3/2}$	1.1	199.8	53.3	0.9	1.9	0.7	13.8
2	${}^2P_{1/2}, \epsilon_{1/2^-}$	1.2	187.7	46.3	1.9	4.9	0.8	13.5
3	${}^4P_{1/2}, \epsilon_{3/2^-}$	1.1	0.6	1.8	1.7	1.2	0.7	1.2
4	${}^4P_{3/2}, \epsilon_{3/2^-}$	1.2	0.5	5.3	2.2	5.7	0.7	2.2
5	${}^4P_{5/2}, \epsilon_{3/2^-}$	1.3	0.5	1.9	0.8	1.8	0.7	1.2
6	${}^2S_{1/2}, {}^4S_{3/2}, {}^2P_J,$ ${}^4P_J, \epsilon_{1/2^-}, \epsilon_{3/2^-}$	1.0	0.8	1.1	0.8	0.9	0.5	0.9

TABLE II. The convergence of the partial wave expansion is indicated by χ_N^2 for different values of L_{max} at $E_{c.m.} = 431.3$ and 667 keV. The number of data points for each observable is shown in parentheses.

L_{max}	χ_N^2						Total
	$\sigma(\theta)$	A_y	iT_{11}	T_{20}	T_{21}	T_{22}	
$E_{c.m.} = 431.3$ keV	(22)	(3)	(3)	(24)	(22)	(20)	(94)
1	8.45	17.97	14.16	42.15	18.08	29.73	24.32
2	2.31	17.58	13.17	1.53	5.40	1.72	3.54
3	1.87	17.62	13.13	1.91	2.61	1.55	2.85
4	1.86	17.62	13.12	1.94	2.61	1.53	2.85
$E_{c.m.} = 667$ keV	(56)	(7)	(8)	(24)	(24)	(24)	(143)
1	49.22	194.82	69.74	118.49	51.34	202.61	95.22
2	1.37	189.92	61.88	2.44	10.98	3.96	16.21
3	1.11	190.43	61.38	1.11	2.83	0.66	13.96
4	1.15	190.46	61.39	0.98	2.52	0.66	13.91

TABLE III. The χ_N^2 calculated for specific trials of the phase-shift analysis at $E_{c.m.} = 431.3$ keV. The number of data points in the angular distribution of each observable is the value in parentheses under the title. The total χ_N^2 is the sum of χ^2 for each observable divided by 94 (the total number of data points).

Trial	Free Parameters	χ_N^2						Total (94)
		$\sigma(\theta)$ (22)	A_y (3)	iT_{11} (3)	T_{20} (24)	T_{21} (22)	T_{22} (20)	
AV18	None	23.2	23.5	19.3	2.9	4.2	2.1	9.0
AV18+UR	None	1.9	17.6	13.1	1.9	2.6	1.5	2.8
1	${}^2P_{1/2}, {}^2P_{3/2}$	1.6	25.1	2.7	1.3	1.1	1.6	2.2
2	${}^2P_{1/2}, \epsilon_{1/2^-}$	1.6	30.1	2.2	1.2	0.9	1.6	2.2
3	${}^4P_{1/2}, \epsilon_{3/2^-}$	1.7	0.9	1.3	1.2	0.9	1.5	1.3
4	${}^4P_{3/2}, \epsilon_{3/2^-}$	1.7	0.5	16.6	2.0	2.5	1.5	2.4
5	${}^4P_{5/2}, \epsilon_{3/2^-}$	2.1	1.4	3.4	1.6	1.9	1.5	1.8
6	${}^2S_{1/2}, {}^4S_{3/2}, {}^2P_J, {}^4P_J, \epsilon_{1/2^-}, \epsilon_{3/2^-}$	1.1	0.3	0.9	1.1	0.8	1.3	1.0

TABLE IV. Phase shifts and mixing parameters obtained from single-energy phase-shift analysis where all S - and P -wave phase-shifts were varied. The first column for each energy contains the values calculated with the AV18 and UR-IX potentials and were the starting values for the analyses. The second column lists the values produced from the fits to the data.

Parameter	$E_{c.m.} = 431.3$ keV		$E_{c.m.} = 667$ keV	
	Calculation($^\circ$)	Fit ($^\circ$)	Calculation($^\circ$)	Fit ($^\circ$)
${}^2S_{1/2}$	-5.811	-7.64 ± 0.74	-10.00	-10.53 ± 0.59
${}^4S_{3/2}$	-28.08	-27.48 ± 0.25	-36.93	-36.81 ± 0.19
${}^2P_{1/2}$	-1.993	-2.17 ± 0.44	-3.339	-2.91 ± 0.15
${}^2P_{3/2}$	-1.975	-1.61 ± 0.28	-3.303	-3.42 ± 0.13
$\epsilon_{1/2^-}$	2.499	1.82 ± 0.46	2.954	3.33 ± 0.13
${}^4P_{1/2}$	5.262	5.06 ± 0.11	9.199	9.18 ± 0.07
${}^4P_{3/2}$	6.127	6.19 ± 0.12	10.69	10.62 ± 0.05
${}^4P_{5/2}$	5.743	5.69 ± 0.10	10.07	10.14 ± 0.04
$\epsilon_{3/2^-}$	-0.886	-1.13 ± 0.29	-1.060	-1.25 ± 0.06

FIGURES

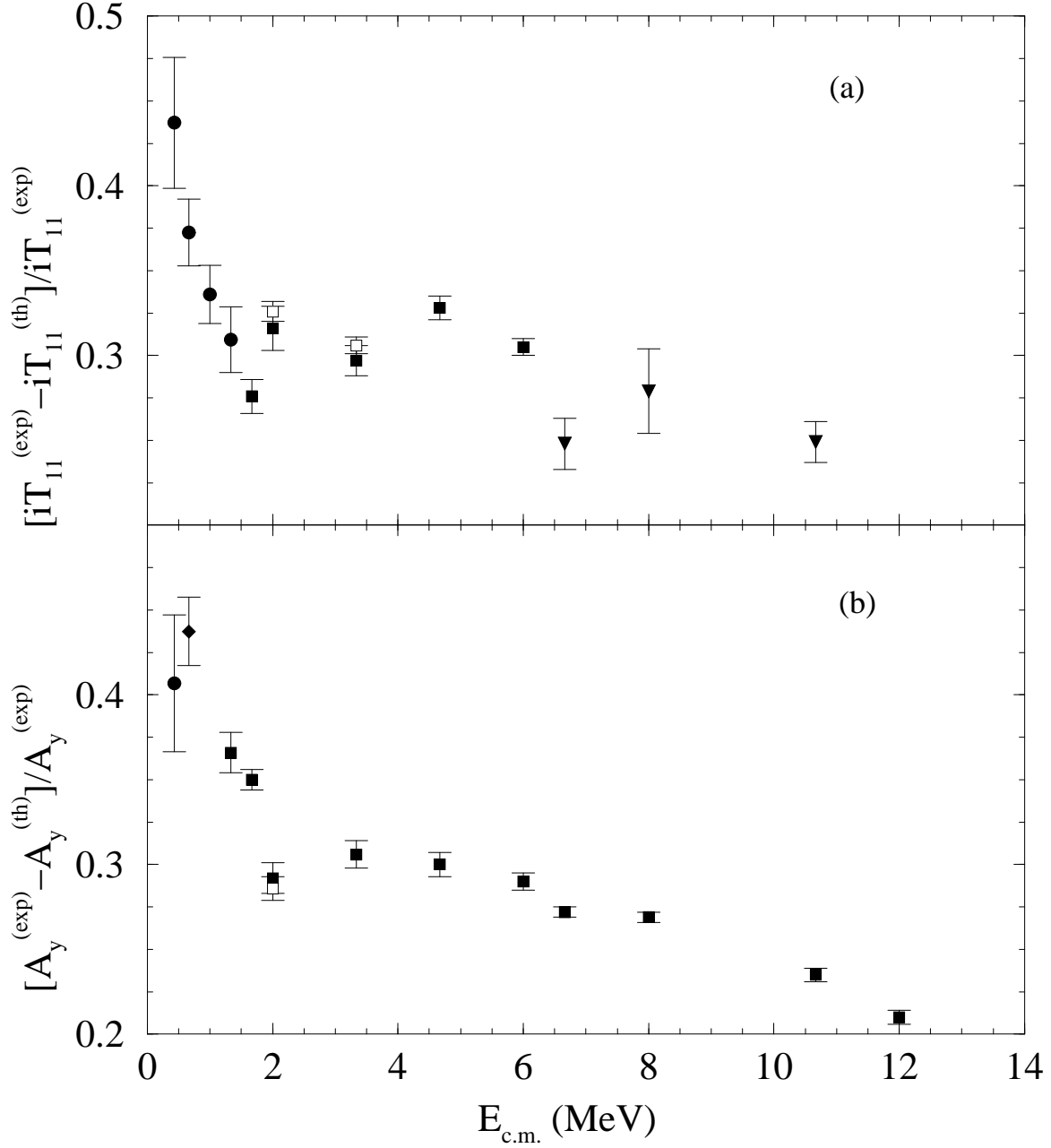


FIG. 1. Differences between experimental data and theoretical calculations using the AV18 potential at the maximum of the angular distributions for (a) iT_{11} and (b) A_y . The points are plotted as the difference between experiment and theory divided by the experimental value. The data are taken from the following sources: Ref. [14,20] (circles), Ref. [12,33,34] (filled squares), Ref. [11,35] (open squares), Ref. [36] (triangles), and Ref. [37] (diamond).

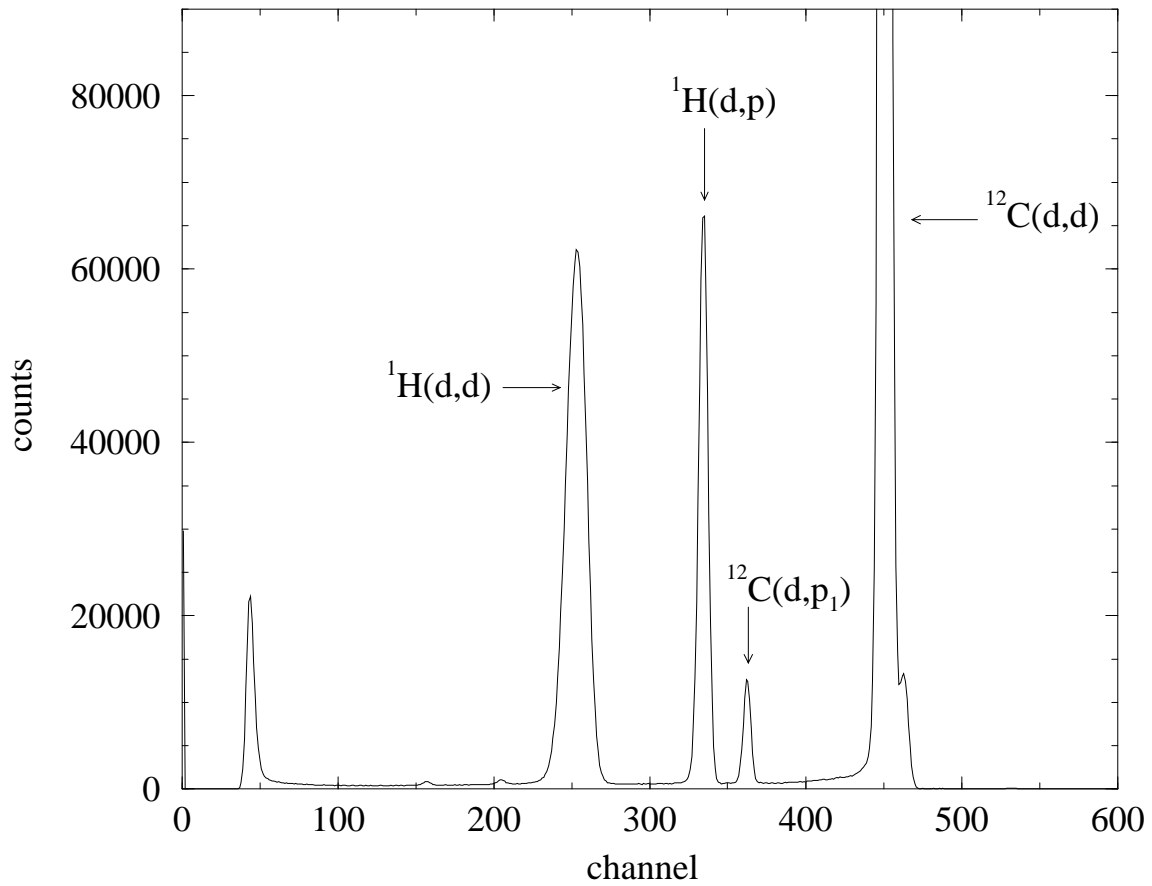


FIG. 2. Typical spectrum for a 2.00 MeV deuteron beam on thin hydrogenated carbon foil. The detectors were positioned at $\theta_{lab} = 26.1^\circ$. In addition to the peak at channel 360, there are two smaller peaks at channels 160 and 210 which arise from $^{12}\text{C}(d,p)^{13}\text{C}$ reactions.

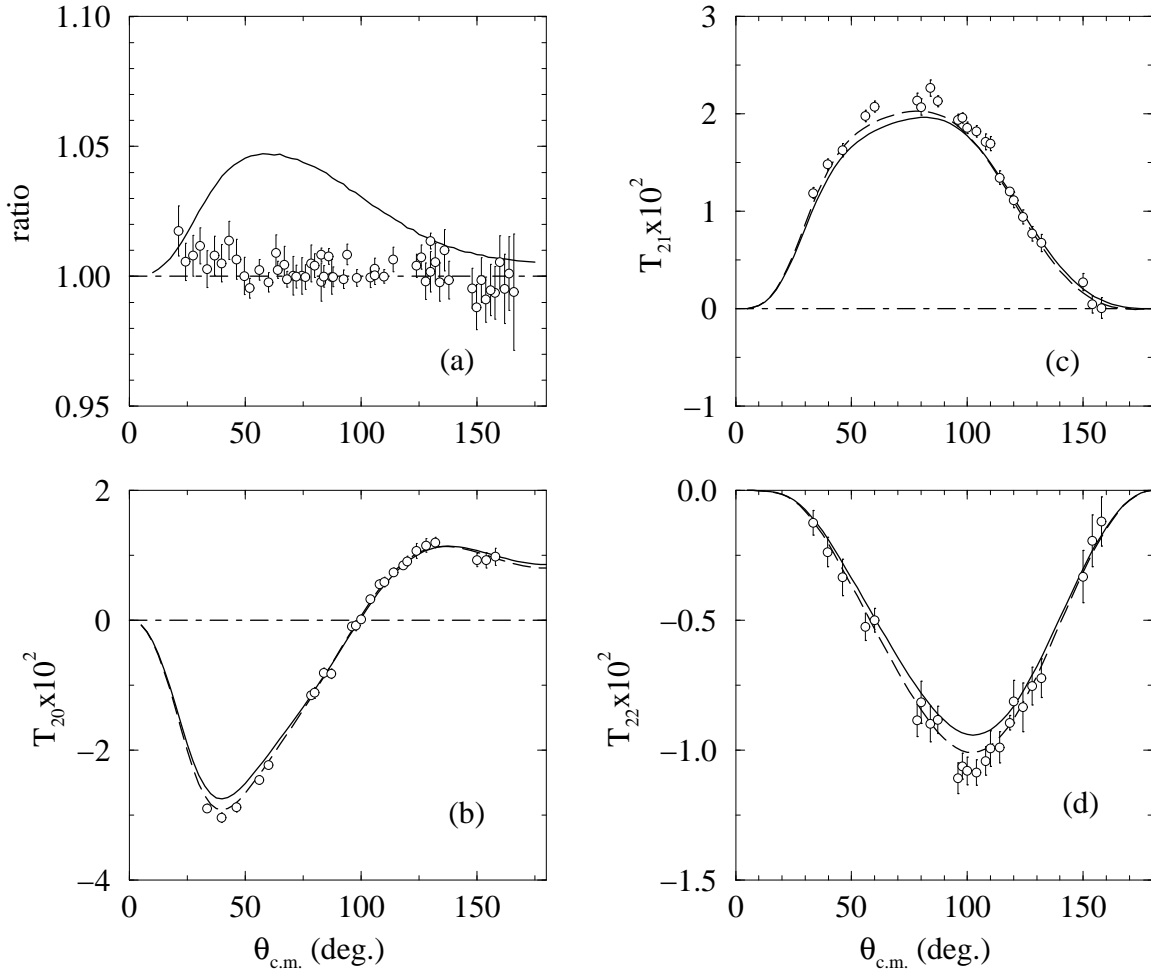


FIG. 3. Angular distributions for p-d elastic scattering at $E_{c.m.} = 667$ keV. Graph (a) shows the ratio of the cross-sections to the AV18+UR-IX calculation. The circles represent the data, including statistical errors, divided by the AV18+UR-IX calculation. The solid line is the ratio of the AV18 calculation to the AV18+UR-IX calculation. Graphs (b), (c), and (d) show the angular distributions of the TAP data. The solid and dashed curves are calculations with the AV18 and AV18+UR-IX potentials, respectively. The dot-dashed line marks zero on these graphs.

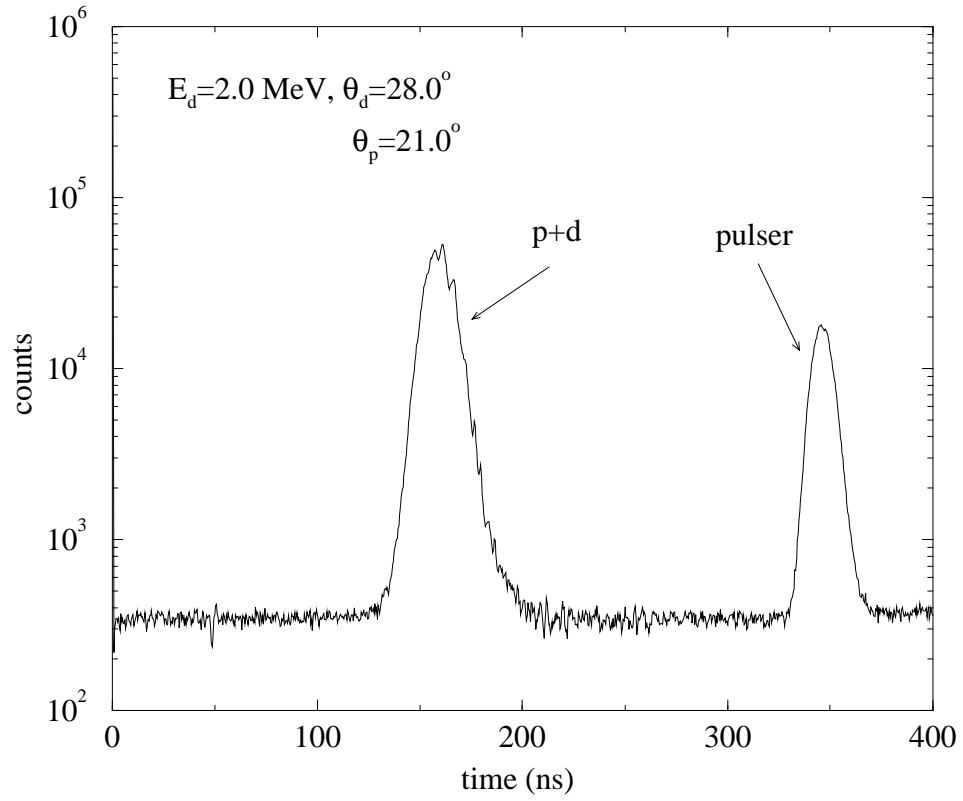


FIG. 4. A proton-duetron time-of-flight spectrum using a four-detector configuration. The time resolution is approximately 20 ns.

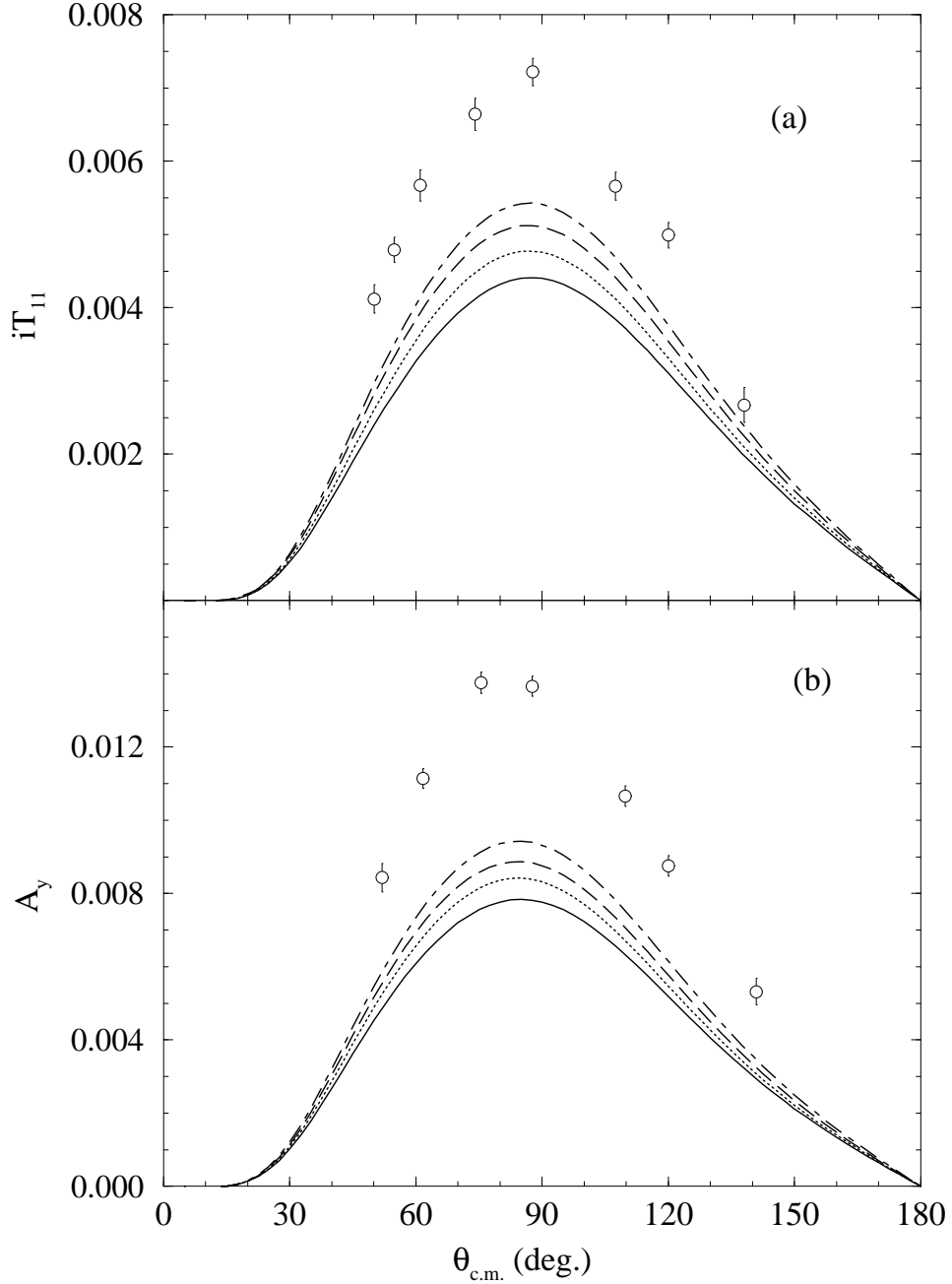


FIG. 5. Angular distributions for iT_{11} and A_y for p-d elastic scattering at $E_{c.m.} = 667$ keV. The errors include the uncertainty in the beam polarization as well as statistical uncertainties. The solid, dashed, and dotted curves are variational calculations with the AV18, AV18+UR-IX, and AV18+TM potentials, respectively. The dot-dashed curve is the calculation with the AV18+TM' potentials.

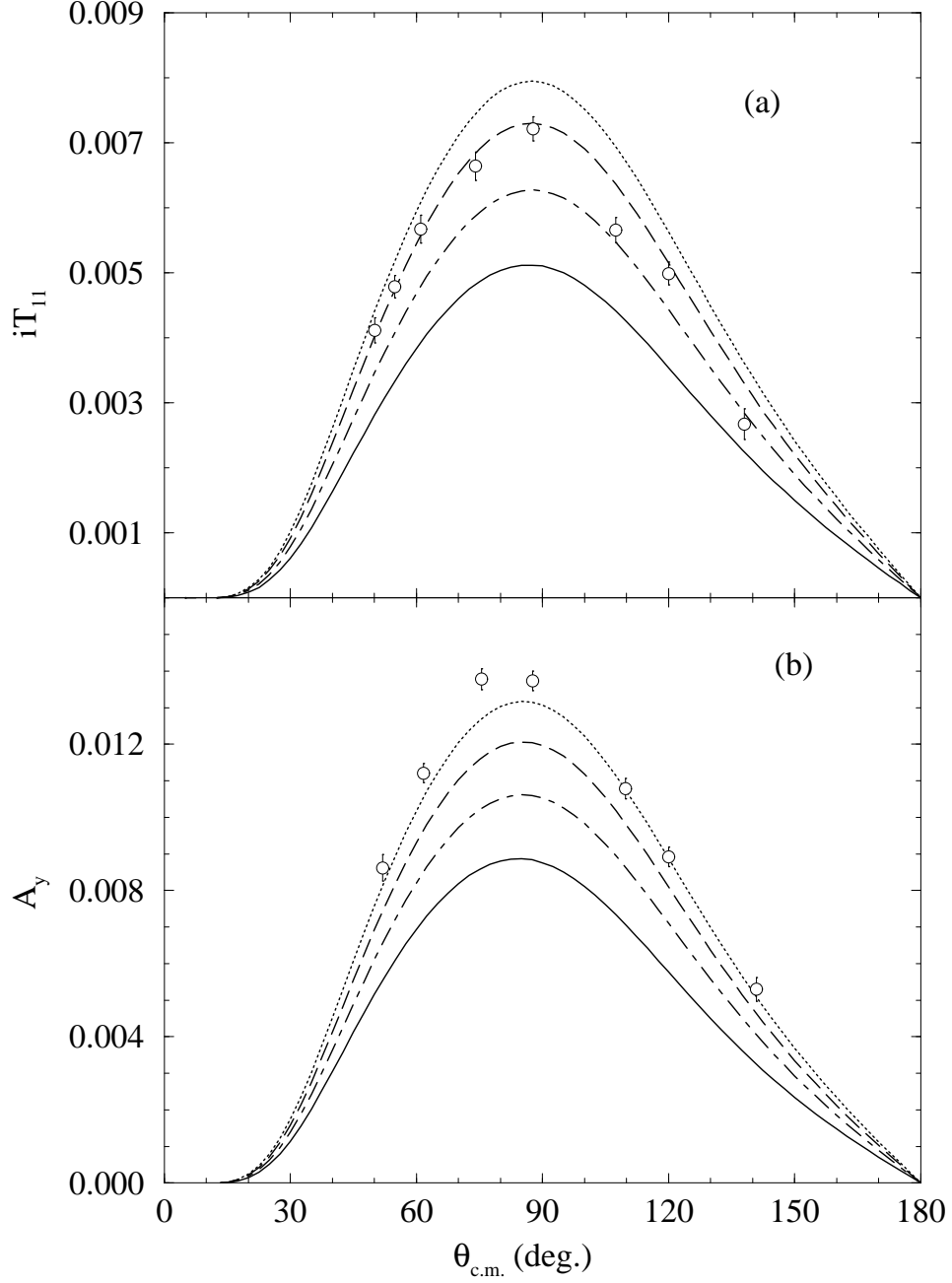


FIG. 6. Comparison between iT_{11} and A_y data and calculations with AV18+UR-IX with the addition of phenomenological spin-orbit forces at $E_{c.m.} = 667$ keV. The solid curve is the calculation without any modifications. The dotted curve represents a long-range interaction ($W_0 = -1$ MeV, $\alpha = 0.7$ fm $^{-1}$), the dashed curve is for a medium-range ($W_0 = -10$ MeV, $\alpha = 1.2$ fm $^{-1}$), and the dot-dashed curve indicates a short-range interaction ($W_0 = -20$ MeV, $\alpha = 1.5$ fm $^{-1}$) [30].